Hindawi
Journal of Advanced Transportation
Volume 2024, Article ID 6632473, 16 pages
https://doi.org/10.1155/2024/6632473

Research Article

Time-Delay following Model for Connected and Automated Vehicles with Collision Conflicts and Forced Deceleration

Wenbo Wang,[1,2] **Fei Hui**,[1,2] **Kaiwang Zhang**,[1] **Xiangmo Zhao**,[1,2] **and Asad J. Khattak**[1,3]

[1]*School of Information Engineering, Chang'an University, Xi'an 710064, China*
[2]*The Joint Laboratory for Internet of Vehicles, Ministry of Education-China Mobile Communications Corporation, Chang'an University, Xi'an 710064, China*
[3]*Department of Civil and Environmental Engineering, University of Tennessee, Knoxville, TN 37996, USA*

Correspondence should be addressed to Fei Hui; feihui@chd.edu.cn

Received 2 March 2023; Revised 14 April 2023; Accepted 20 March 2024; Published 12 April 2024

Academic Editor: Bo Leng

The connected and automated car-following model can provide a model reference for the queue control algorithm of connected and automated driving and has become a hot research topic in the field of connected vehicles and intelligent transportation. A queue of fast-moving vehicles on urban roads can cause traffic congestion when forced to slow down and, in serious cases, can cause rear-impact accidents. Therefore, this paper introduces information on the time delay of information reception and processing, a collision risk quantification factor reflecting the speed characteristics of the front vehicle, and the speed limit and proposes an improved intelligent driver collision quantification model that considers drastic changes in the speed of the front vehicle. Additionally, the model parameters are calibrated using real vehicle data from urban roads combined with an improved salp swarm algorithm. Finally, the evolution rule of disturbance in the traffic flow under different states is analyzed using a time-space diagram, and the DIDM-CSCL model is compared with the classical IDM. The results show that the improved IDM can better describe the following behavior at the microscopic level, which provides a basis for research related to connected and automated driving.

1. Introduction

Following behavior is a result of the interaction of various elements of a particular driver-vehicle-environment aggregation and describes the various states of affairs between two adjacent vehicles in a one-way lane where overtaking is restricted. Following theory is a microscopic traffic flow theory that analyzes the efficiency and stability of vehicle operations by describing the following behavior of vehicles and using the driving characteristics of non-free-running convoys [1]. The study of vehicle-following behavior from different perspectives and modeling ideas based on following theory is an important area of research in microscopic traffic flow simulation. Based on their development over time, car-following models are mainly divided into the following groups: Gazis et al. [2] proposed the general expression of the classical GM car-following model based on the stimulus-response principle; Kometani and Sasaki [3] proposed a safety distance model considering the safety distance of the car following; Michaels [4] put forward a physiology-psychology model by defining a series of thresholds and expected distances to reflect people's feelings and reactions; Kikuchi and Chakraborty [5] used artificial intelligence technology to directly find the rules of car-following behavior from track data and formed an artificial intelligence model; Bando et al. [6] established an optimized speed model by using information such as the speed of the vehicle in front and distance between vehicles. However, with the continuous improvement of intelligent driving systems, V2V and V2I technologies, with the installation of devices such as ADAS, AEBS, LIDAR, and GPS, vehicles are able to access increasingly more accurate real-time data of the surrounding driver-vehicle-environment network connection and thus enable alerting, assistance, and intelligent

decision-making functions for driving operations [7]. Figure 1 shows the development process of the main car-following model. Some scholars have improved the traditional car-following model to suit the needs of models for connected and automated vehicles in complex environments.

Treiber et al. [8] succeeded in obtaining an intelligent driver model (IDM) with only a few physically meaningful parameters that are easy to calibrate, based on the assumption of reasonable conditions and the reproduction of realistic bottlenecks, using simulations of real highway traffic congestion data (e.g., entrance ramps, lane closures, or uphill ramps) in a quantitative manner with boundary conditions. The model has a stable and smooth transition of controlled acceleration, deceleration, and braking in describing the following behavior and can describe different states from free flow to fully congested flow with a unified model. Subsequently, different scholars have explored the IDM mainly from the perspective of human-vehicle driving characteristics and from the perspective of intelligent driving technology.

In terms of research and improvement of the IDM based on traditional human-vehicle driving characteristics, the following characteristics were analyzed by considering factors such as anticipatory behavior, limited reaction time, driving task difficulty, and driving style. Chen et al. [9] added two factors, the multianticipative behaviors and reaction delays of drivers, to the classical IDM model and constructed a multianticipation intelligent driver model (MIDM) by considering the intervehicle distance information and speed difference information of neighboring vehicles. The results show that the MIDM can maintain the stability of homogeneous motorway traffic flow in the presence of small disturbances. Treiber et al. [10] developed a human driver model (HDM) that is consistent with empirical data on high-speed traffic, considering finite reaction times, estimation errors, and temporal anticipation. The fitting results show that the HDM can compensate for the unstable effects of reaction times and estimation errors by reducing the transition gradient between free traffic and congested traffic, thus increasing the wavelength of vehicles stopping. Hoogendoorn et al. [11] and Saifuzzaman and Zheng [12] incorporated the task-capability-interface (TCI) model proposed by Fuller [13] into the IDM to capture the compensatory effects of driver distraction. Saifuzzaman et al. [14] developed a task difficulty intelligent driver model (TDIDM) based on human behavioral factors by measuring the interaction state between driving task demands and driving ability as driving task difficulty. The numerical simulation results show that the TDIDM can effectively control the following behavior of the subject vehicle under different driving task difficulties and maintain a relatively smooth following speed after the driving task requirements are accurately obtained. However, most of the above models lack real vehicle tracking data or the model parameters are not calibrated, and a small number of models have validation data from high-speed road sections and lack urban tracking data for parameter calibration and validation. Therefore, the ability of the IDM to control the following behavior on urban roads needs to be further confirmed.

In the research and improvement of the IDM based on connected and automated driving technology, the following characteristics were analyzed by considering factors such as multivehicle information for connected vehicles and intelligent driving systems. Xiao et al. [15] considered the conditional heteroskedasticity of acceleration fluctuations between vehicles in following behavior and developed an IDM-GARCH model by combining the dynamic balance of efficiency drivers and safety drivers. The model was more accurate in predicting the value of changes in vehicle acceleration and occurrence of risky driving behavior. Zong et al. [16] developed a multifront and rear IDM suitable for describing the behavior of connected and automated vehicles, considering factors such as multivehicle information and time delay. The simulation results showed that temporarily formed vehicle queues can interact and make decisions about their respective driving trends in real time while driving by receiving effective information from the front and rear vehicles, improving the operational efficiency, comfort, and stability of the traffic flow. Sharma et al. [17] incorporated driver compliance behavior into a connected vehicle driving strategy, combining prospect theory and weighting functions to design a CVDS-IDM based on low- and high-compliance behavior to determine the level of compliance in terms of time headway. The calibration results showed that driver behavior is safer and more efficient in a connected environment. Li et al. [18] proposed an improved intelligent driver model (MIDM) based on the driver's responsiveness to speed differences and safety information combined with the dynamic characteristics of connected vehicles. The test results showed that the improved model can contribute to the stability of the traffic flow and improve the operational efficiency of the fleet by obtaining effective information on the following vehicles. However, the above improved model does not consider the possibility of collision scenarios occurring in the following behavior exacerbated by the speed fluctuations generated by the subject vehicle when there are large fluctuations in the speed of the front vehicle. Therefore, quantitative factors of collision risk related to the speed of the front vehicle in a connected environment are introduced into the IDM, and appropriate weights are set to control the behavior of the vehicle.

In the above studies on the modeling of following behavior, there were few studies on the influence of real-time speed information and quantitative crash risk factors on the following behavior of the front vehicle. Some scholars have found that drivers have different requirements for the desired headway under different road conditions because of speed restrictions and other factors [19, 20]. Furthermore, in addition to the need to calibrate the improved IDM parameters using urban road traffic following data, the solution accuracy and convergence rate of the parameter optimization must also be considered. In this study, an improved DIDM-CSCL model is constructed based on the analysis of vehicle-following behavior, which takes into account information such as the time delay of information reception and processing, the collision risk quantification factor reflecting the speed

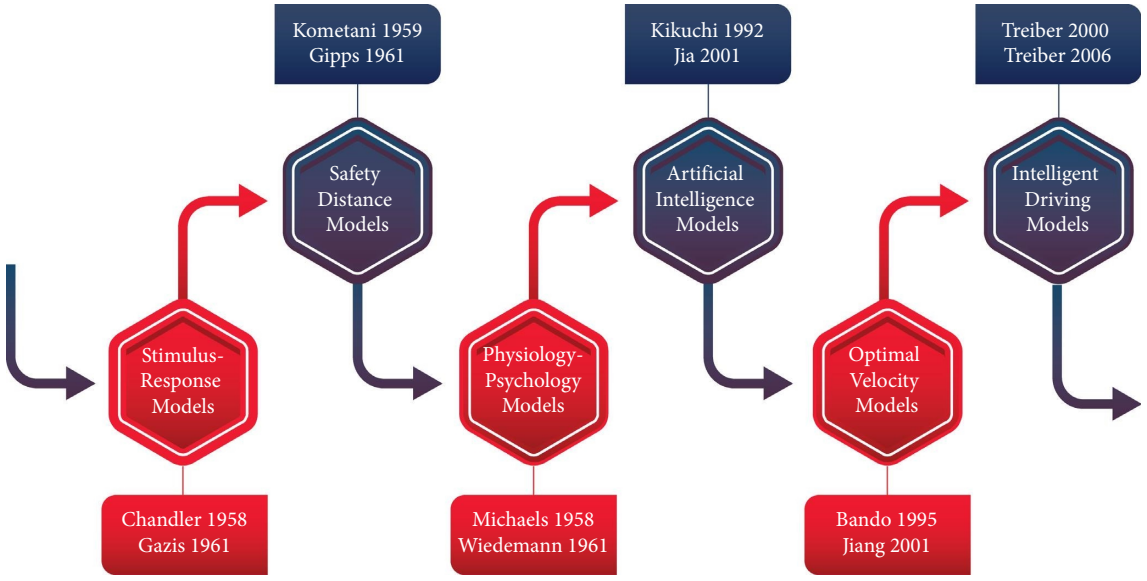

Figure 1: Development process of the main car-following models.

characteristics of the vehicle in front, and the speed limits. The relevant parameters in the model were calibrated using real vehicle data from urban roads and an improved salp swarm algorithm. By introducing specific driver-vehicle-environment target state information, the stability of the subject vehicle driving in the following behavior is improved. In particular, it is potentially useful for temporary queues consisting of AVs to improve the stability and operational efficiency of the queue and overall traffic flow.

The remainder of this paper is organized as follows. The DIDM-CSCL model is constructed in Section 2, and in Section 3, the proposed model is analyzed for stability and compared with the IDM. The parameter calibration and algorithm search are presented in Section 4, numerical simulations are presented in Section 5, and conclusions are presented in the last section.

2. Methodology

The classical IDM was proposed by Treiber et al. [8, 21] as an intelligent driving model based on generalized following behavior characteristics (vehicles always try to maintain the desired speed and headway spacing, etc.), including the tendency to react to acceleration and deceleration movements in free flow and congested flow states. Its formula is as follows:

$$\begin{aligned} a_n(t) &= \frac{\mathrm{d}v_n(t)}{\mathrm{d}t} \\ &= a_0\left(1-\left(\frac{v_n(t)}{v_0}\right)^4-\left(\frac{s_n^*(t)}{s_n(t)}\right)^2\right), \end{aligned} \tag{1}$$

$$s_n^*(t) = s_0 + Tv_n(t) + \frac{v_n(t)\Delta v(t)}{2\sqrt{a_0 b}}, \tag{2}$$

where a_0 and v_0 are the maximum acceleration and desired speed of the nth vehicle in the free flow, respectively, $v_n(t)$ is the speed of the following vehicle at time t, $s_n^*(t)$ is the desired gap, s_0 is the minimum gap, T is the safe time headway, $\Delta v(t)$ is the speed difference between the following vehicle and the front vehicle, and b is the comfortable deceleration.

In equation (1), the acceleration in the IDM at a given moment is related to the current speed of the vehicle, time headway, and speed difference with the vehicle ahead. However, in practical studies, it has been found that the speed difference in the IDM does not fit the acceleration with the corresponding effect well when road traffic obstruction causes a large change in the speed of the vehicle ahead, thus reducing the safety of the following behavior [22]. Moreover, speed limits are an important factor in causing road traffic congestion, significantly influencing the choice of the desired following distance of the rear driver. However, previous studies have shown that considering safety factors related to crash expectations can effectively enhance traffic flow stability. Li et al. [23] considered the time-exposed time-to-collision (TET) and the time integrated time-to-collision (TIT) as vehicle safety factors and developed a crash assessment model. The results showed that the model could significantly reduce the risk of highway vehicle collisions with a reasonable time headway and time delay. Wu et al. [24] used time-to-collision at braking (TTC-brake) and total travel time (TTT) as evaluation indexes for the risk assessment of collisions at highway bottlenecks under foggy conditions and effectively performed a risk assessment of the following model and control strategy.

The most common traffic accidents during the following behavior are rear-end accidents [25]. In reality, it is not possible to measure crash expectations in an extreme way (e.g., the number of collisions and injury severity); therefore, alternative safety measures are used to establish the relationship between risk and vehicle travel variables. In

previous studies, different scholars have proposed several valid crash expectation metrics, one of which is time-to-collision (TTC) [26]. TTC represents the time it takes for two vehicles to collide when the primary vehicle and the vehicle in front travel in the same lane while maintaining the existing speed. TTC is currently available in several ways, either by means of intelligent driver assistance systems (e.g., FCW and AEB) or by real-time interaction with information on the motion of the following vehicle in a connected environment [27–29].

$$\mathrm{TTC}_n(t) = \begin{cases} \dfrac{x_{n-1}(t) - x_n(t) - l}{v_n(t) - v_{n-1}(t)}, & v_n(t) > v_{n-1}(t), \\ \infty, \quad \text{otherwise.} \end{cases} \tag{3}$$

It is deformed and transformed into the collision risk quantification factor:

$$\begin{aligned} \mathrm{CSC} &= -\frac{1}{\mathrm{TTC}_n(t)} \\ &= \frac{v_{n-1}(t) - v_n(t)}{x_{n-1}(t) - x_n(t) - l}. \end{aligned} \tag{4}$$

When the speed of the vehicle in front is less than the speed of the vehicle behind it, a collision may occur, requiring a slowdown.

$$\mathrm{CSC} = \frac{v_{n-1}(t) - v_n(t)}{x_{n-1}(t) - x_n(t) - l} < 0. \tag{5}$$

When the speed of the preceding vehicle is equal to that of the following vehicle, it may continue to travel at a constant speed.

$$\mathrm{CSC} = \frac{v_{n-1}(t) - v_n(t)}{x_{n-1}(t) - x_n(t) - l} = 0. \tag{6}$$

When the speed of the vehicle in front is greater than the speed of the vehicle behind it, it is possible to accelerate moderately.

$$\mathrm{CSC} = \frac{v_{n-1}(t) - v_n(t)}{x_{n-1}(t) - x_n(t) - l} > 0. \tag{7}$$

In this study, as shown in Figure 2, it is assumed that all vehicles are fitted with a complete automation system, including hardware and software units, as well as a V2V onboard unit for information transfer. In this way, each vehicle can obtain information about the surrounding vehicles with the help of the connected devices, and in turn, all vehicles can react automatically based on the above information. For example, by accelerating and decelerating to follow the preceding vehicles, each vehicle can maintain a safe distance and emergency avoidance. Moreover, the speed limit is used as a constraint [30] to verify the synergy and transferability of the model. Therefore, we develop a descriptive and empirical car-following model with linear combination of CSC and speed limit as shown in (8) and (9).

Converting equation (1) into the DIDM-CSCL mode yields

$$\frac{\mathrm{d}v_n(t + t_d)}{\mathrm{d}t} = a_0\left(1 - \left(\frac{v_n(t)}{v_0}\right)^4 - \left(\frac{s_n^*(t)}{s_n(t)}\right)^2\right) + \gamma \mathrm{CSC} v_{n-1}(t) + \mu\left(v_{\lim} - v_n(t)\right), \tag{8}$$

where t_d is the time delay for message reception and processing, $v_{\lim}$ is the speed limit information, γ denotes the collision quantization sensitivity factor, and μ denotes the sensitivity factor for the speed limits.

Substitute into equation (4) and simplify to obtain the DIDM-CSCL model as

$$\frac{\mathrm{d}v_n(t + t_d)}{\mathrm{d}t} = a_0\left(1 - \left(\frac{v_n(t)}{v_0}\right)^4 - \left(\frac{s_n^*(t)}{s_n(t)}\right)^2\right) - \gamma \frac{\Delta v(t)}{s_n(t)} v_{n-1}(t) + \mu\left(v_{\lim} - v_n(t)\right), \tag{9}$$

where $s_n(t) = x_{n-1}(t) - x_n(t) - l$ is the actual gap.

The above model can be used to explore the effect of the additional term on the speed and the effect of speed limits by varying the weights γ and μ to improve the stability of the traffic flow under disturbances.

3. Stability Analysis

Stability analysis is an important part of this following model. Sun et al. [31] analyzed the local and string stability of car-following models with different characteristics using methods based on the characteristic equation and Lyapunov criterion, compared the stability criteria of some methods using the principles of consistency and applicability, and investigated the effects of connectivity and time delay on the stability of the model. Montanino and Punzo [32] proposed a string stability modeling method that considers driver and vehicle heterogeneity by classifying the stability correlates of the following model into system type, domain of action, etc., and using the L2 induced paradigm as a stability metric. Sun et al. [33] combined the string stability of car-following and traffic flow oscillations by analyzing the instability factors of

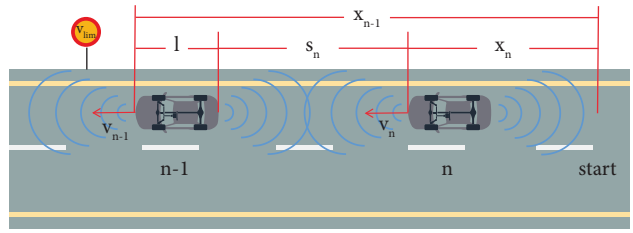

Figure 2: Schematic diagram of the DIDM-CSCL model.

single-vehicle travel in the following behavior and the oscillation criterion in queue marching to complementarily achieve the compressing and alleviating of traffic congestion. In this study, the stability of the DIDM-CSCL model is analyzed using the linear stability theory, and equation (10) is simplified as follows:

$$\frac{\mathrm{d}v_n(t+t_d)}{\mathrm{d}t} = f_n\left(s(t), v_n(t), \Delta v(t), v_{n-1}(t)\right). \tag{10}$$

We assume that $\bar{s}$ is the average time headway of adjacent vehicles in a uniform flow. $\bar{v}$ is the speed of vehicles in a uniform flow, and in the initial state, all vehicles travel at the same headway and at the same speed. The vehicle positions in the uniform flow are

$$\bar{x}_n(t) = (N-n)\bar{s} + \bar{v}t, \quad n = 1, 2, 3..., N. \tag{11}$$

Assuming that $y_n(t)$ is the disturbance generated by vehicle n at time t, the disturbance is added to equation (11).

$$y_n(t) = \mathrm{c}e^{i\alpha_k n + \mathrm{z}t} = x_n(t) - \bar{x}_n(t), \quad y_n(t) \longrightarrow 0, \tag{12}$$

where $\alpha_k = 2\pi k/N$ $(k = 0, 1, ..., N-1)$ is a constant. Taking the second derivative of both sides of equation (12) yields

$$\mathrm{y}_n''(t+t_d) = x_n''(t+t_d) - \bar{x}_n''(t+t_d) = \frac{\mathrm{d}v_n(t+t_d)}{\mathrm{d}t}. \tag{13}$$

Substituting equation (10) into equation (13) gives

$$y_n''(t+t_d) = f_n\left(s(t), v_n(t), \Delta v(t), v_{n-1}(t)\right). \tag{14}$$

Linearizing equation (14) gives

$$\begin{aligned} y_n''(t+t_d) = {} & f_n^s\left(y_{n-1}(t) - y_n(t)\right) + f_n^{v_n} y_n'(t) \\ & + f_n^{\Delta v}\left(y_n'(t) - y_{n-1}'(t)\right) + f_n^{v_{n-1}} y_{n-1}'(t), \end{aligned} \tag{15}$$

where $f_n^s = (\partial f_n/\partial s)|_{\bar{v},\bar{s}} \geq 0$, $f_n^{v_n} = (\partial f_n/\partial v_n)|_{\bar{v},\bar{s}} \leq 0$, $f_n^{\Delta v} = (\partial f_n/\partial \Delta v)|_{\bar{v},\bar{s}} \leq 0$ and $f_n^{v_{n-1}} = (\partial f_n/\partial v_{n-1})|_{\bar{v},\bar{s}} \geq 0$.

Rewriting equation (15) using the Taylor series expansion and the first order derivative formula yields the difference equation.

$$\begin{aligned} y_n'(t+2t_d) - y_n'(t+t_d) = {} & t_d f_n^s\left(y_{n-1}(t) - y_n(t)\right) + f_n^{v_n}\left(y_n(t+t_d) - y_n(t)\right) \\ & + f_n^{\Delta v}\left(y_n(t+t_d) - y_n(t) - y_{n-1}(t+t_d) + y_{n-1}(t)\right) + f_n^{v_{n-1}}\left(y_{n-1}(t+t_d) - y_{n-1}(t)\right). \end{aligned} \tag{16}$$

Substituting $y_n(t) = \mathrm{c}e^{i\alpha_k n + \mathrm{z}t}$ and $y_n'(t) = \mathrm{z}\mathrm{c}e^{i\alpha_k n + \mathrm{z}t}$ into equation (16) and simplifying give

$$\left(e^{\mathrm{z}t_d} - 1\right)\left[\mathrm{z}e^{\mathrm{z}t_d} - f_n^{v_n} - f_n^{\Delta v}\left(1 - e^{-i\alpha_k}\right) - f_n^{v_{n-1}} e^{-i\alpha_k}\right] = t_d f_n^s\left(e^{-i\alpha_k} - 1\right). \tag{17}$$

Substitute the following power series expansions for the parameters in equation (17).

$$z = z_1(i\alpha_k) + z_2(i\alpha_k)^2 + \cdots, \tag{18}$$

$$e^{\mathrm{z}t_d} = 1 + t_d z + \frac{t_d^2 z^2}{2} + \cdots, \tag{19}$$

$$e^{-i\alpha_k} = 1 - i\alpha_k + \frac{(i\alpha_k)^2}{2} - \cdots, \tag{20}$$

where z is the complex growth rate and z_1 and z_2 are real numbers. Expanding this gives the first and second order expressions for z:

$$\left(z_1(i\alpha_k)+z_2(i\alpha_k)^2+\frac{t_d}{2}\left(z_1(i\alpha_k)+z_2(i\alpha_k)^2\right)^2\right)\times\left[z_1(i\alpha_k)+z_2(i\alpha_k)^2+t_d\left(z_1(i\alpha_k)+z_2(i\alpha_k)^2\right)^2\right.$$
$$\left.+\frac{t_d^{\,2}}{2}\left(z_1(i\alpha_k)+z_2(i\alpha_k)^2\right)^3-f_n^{v_n}-f_n^{\Delta v}\left(i\alpha_k-\frac{(i\alpha_k)^2}{2}\right)-f_n^{v_{n-1}}\left(1-i\alpha_k+\frac{(i\alpha_k)^2}{2}\right)\right]=-f_n^s\left(-i\alpha_k+\frac{(i\alpha_k)^2}{2}\right). \tag{21}$$

And thus yields

$$z_1=\frac{f_n^s}{f_n^{v_n}+f_n^{v_{n-1}}} \tag{22}$$

$$z_2=\frac{z_1^{\,2}\left(1-(t_d/2)f_n^{v_n}-(t_d/2)f_n^{v_{n-1}}\right)-z_1\left(f_n^{\Delta v}-f_n^{v_{n-1}}\right)-(1/2)f_n^s}{f_n^{v_n}+f_n^{v_{n-1}}}. \tag{23}$$

Traffic flows become unstable when $z_2<0$ is subjected to small perturbations and stabilize when $z_2>0$ is perturbed. The stability condition is

$$\left(\frac{f_n^s}{f_n^{v_n}+f_n^{v_{n-1}}}\right)^2\left(1-\frac{t_d}{2}f_n^{v_n}-\frac{t_d}{2}f_n^{v_{n-1}}\right)-\left(\frac{f_n^s}{f_n^{v_n}+f_n^{v_{n-1}}}\right)\left(f_n^{\Delta v}-f_n^{v_{n-1}}\right)-\frac{1}{2}f_n^s<0. \tag{24}$$

Simplifying and moving the terms give

$$\frac{t_d}{2}<\frac{1}{f_n^{v_n}+f_n^{v_{n-1}}}-\frac{2f_n^{\Delta v}+f_n^{v_n}-f_n^{v_{n-1}}}{2f_n^s}. \tag{25}$$

The expressions for f_n^s, $f_n^{v_n}$, $f_n^{\Delta v}$, and $f_n^{v_{n-1}}$ can be obtained from equation (25) as follows:

$$f_n^s=\frac{2a_0}{s_n(t)}\left(\frac{s_0+Tv_n(t)+\left(v_n(t)\Delta v/2\sqrt{a_0b}\right)}{s_n(t)}\right)^2+\gamma\frac{\Delta v}{s_n^2(t)}v_{n-1}(t), \tag{26}$$

$$f_n^{v_n}=-2a_0\left(\frac{2}{v_0}\left(\frac{v_n(t)}{v_0}\right)^3+\frac{\left(T+\left(\Delta v/2\sqrt{a_0b}\right)\right)\left(s_0+Tv_n(t)+\left(v_n(t)\Delta v/2\sqrt{a_0b}\right)\right)}{s_n^2(t)}\right)-\mu, \tag{27}$$

$$f_n^{\Delta v}=\frac{\left(s_0+Tv_n(t)+\left(v_n(t)\Delta v/2\sqrt{a_0b}\right)\right)v_n(t)}{s_n^2(t)}\sqrt{\frac{a_0}{b}}-\gamma\frac{v_{n-1}(t)}{s_n(t)}, \tag{28}$$

$$f_n^{v_{n-1}}=-\gamma\frac{\Delta v}{s_n(t)}. \tag{29}$$

Substituting equations (26)–(29) into equation (25), the stability condition is obtained as

$$\frac{t_d}{2} < \frac{1}{-2a_0\left((2/v_0)(v_n(t)/v_0)^3 + \left(T(s_0 + Tv_n(t))/s_n^2(t)\right)\right) - \mu} - \frac{\left((s_0 + Tv_n(t))v_n(t)/s_n^2(t)\right)\sqrt{(a_0/b)} - -\gamma\left(v_{n-1}(t)/s_n(t)\right) - a_0\left((2/v_0)(v_n(t)/v_0)^3 + \left(T(s_0 + Tv_n(t))/s_n^2(t)\right)\right) - \mu}{(2a_0/s_n(t))(s_0 + Tv_n(t)/s_n(t))^2}, \tag{30}$$

where $s_n(t)$ is the actual gap of vehicles in homogeneous traffic flow.

Based on equation (30), the stability curves of the model were obtained. Figure 3 shows the stability curves when $t_d = 0$ and $t_d = 0.15$ [34] are set with different parameters γ and μ, where $a_0 = 2$, $v_0 = 10$, $s_0 = 2.5$, $b = 1.5$, and $v_{\lim} = 10$. As γ and μ increase, the stability curve gradually decreases, which indicates that considering the collision risk quantification factor and road speed limits can effectively improve the stability of traffic flow. It can also be noticed that the instability region for $t_d = 0.15$ is significantly larger than that for $t_d = 0$, as the reaction time delays the vehicle's response, thus changing the vehicle's motion.

4. Calibration

For calibration, the optimal set of IDM and their improved model parameters are generally solved using a genetic algorithm (GA) [10], which is a simple and extensible process. However, in the actual calibration process, it is found that when using the GA for global searches at larger population sizes, it is unavoidable to repeatedly fall into local minima or boundary values, which does not meet the demand for solving the optimal solution for the calibration of the parameters of the car-following model. Therefore, in this study, the parameters of the DIDM-CSCL model were calibrated using actual tracking data during the acceleration and deceleration of vehicles on urban roads, and the optimal solution for each parameter was determined using an improved salp swarm algorithm (SSA).

4.1. Improved SSA. SSA is a novel intelligent optimization algorithm proposed by Mirjalili et al. [35] that models the common chain behavior of leaders and followers in a salp swarm chain. The algorithm performs a global exploration and local search by the leader and followers, respectively, during each iteration, effectively reducing the number of cases of falling into the local optima. The completely random population initialization process is shown in the following equation:

$$X_{N\times D} = rand(N, D) \times (ub(N, D) - lb(N, D)) + lb(N, D), \tag{31}$$

where the search space is $N \times D$, N is the population size, and D is the spatial dimension. The upper bounds of the search space are $ub(N, D)$, and the lower bounds are $lb(N, D)$.

During the movement and foraging of the salp swarm chain, the leader's position updates are expressed as

$$X_d^1 = \begin{cases} F_d + c_1\left[(ub_d - lb_d)c_2 + lb_d\right] c_3 \geq 0.5, \\ F_d - c_1\left[(ub_d - lb_d)c_2 + lb_d\right] c_3 < 0.5. \end{cases} \tag{32}$$

$$c_1 = 2e^{-(4l/L)^2}, \tag{33}$$

where $d = 1, 2, 3, \cdots, D$; F_d denotes the position of the food source in the dth dimension; c_2 and c_3 are random numbers on $[0, 1]$; l and L represent the current and maximum number of iterations, respectively. c_1 is a decreasing and then increasing weight, which has a greater impact on the convergence of the algorithm and has the ability to balance the exploration and development of the algorithm.

The follower's position update is represented as

$$X_d^I = \frac{\mathrm{at}^2}{2} + v_0 t + X_d^i, \tag{34}$$

$$a = \frac{(v - v_0)}{t}, \tag{35}$$

$$v = \frac{\left(X_d^{i-1} - X_d^i\right)}{t}, \tag{36}$$

where $i = I = 2, 3, 4, \cdots, N$; a and v represent acceleration and velocity, respectively, v_0 denotes initial velocity, and t is the difference in the number of iterations. X_d^i is the position of the ith follower in dimension d before the update, and X_d^I is the position of the follower after the update. When $t = 1$ and $v_0 = 0$, equation (34) is substituted into equation (36).

$$X_d^I = \frac{\left(X_d^{i-1} + X_d^i\right)}{2}. \tag{37}$$

However, SSA suffers from poor population diversity and slow convergence when faced with numerous complex multidimensional optimization problems [36]. To further improve the convergence speed and solution accuracy of SSA for the estimation of the parameters of the car-following model, this paper introduces circle chaotic mapping to make the algorithm jump out of the local optimum and then explores the search space thoroughly with a higher probability of improving its convergence speed. However, it was found that the circle chaotic mapping cannot obtain

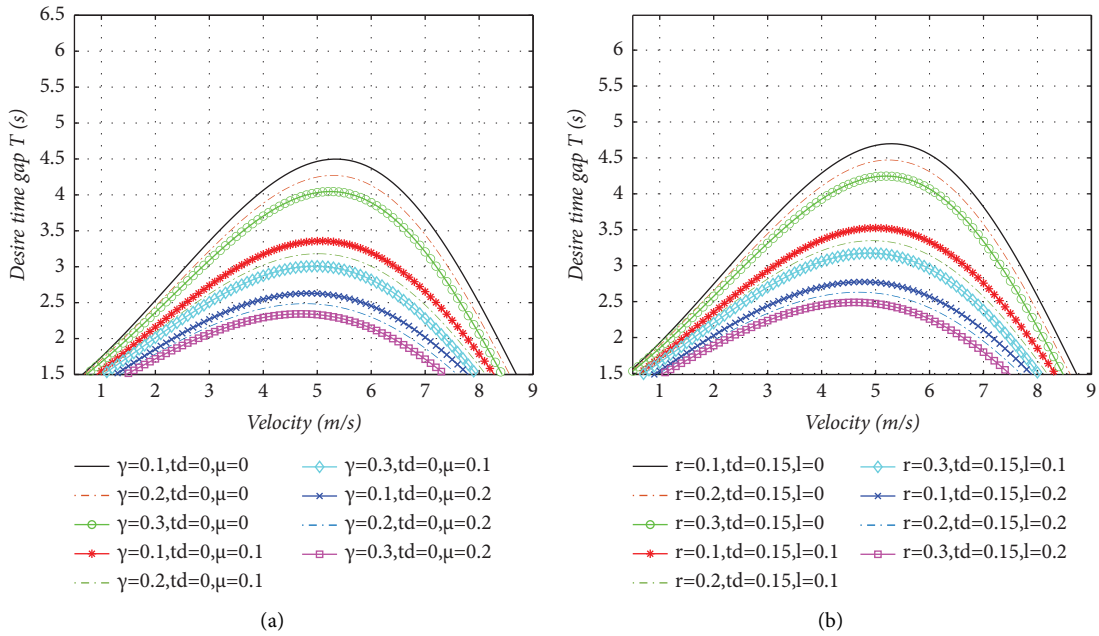

Figure 3: Stability curves at $t_d = 0$ and $t_d = 0.15$ for different γ and μ. (a) $t_d = 0$. (b) $t_d = 0.15$.

a uniformly distributed initial solution in the solution process, and thus, the circle chaotic mapping is improved.

The original circle chaotic mapping formula is

$$Y_{k+1}^n = \mathrm{mod}\left(X_k^n + 0.2 - \left(\frac{0.5}{0.2\pi}\sin\left(2\pi \cdot X_k^n\right)\right), 1\right). \tag{38}$$

The improved logistic-circle chaotic mapping formula is

$$Y_{k+1}^n = \begin{cases} \mathrm{mod}\left(7.7X_k^n + 0.8 - \left(\frac{1.4}{7.7\pi}\sin\left(7.7\pi \cdot X_k^n\right)\right), 1\right), \text{if } X_k^n < 0.5, \\ \mathrm{mod}\left(7.7X_k^n + 0.8 - \left(\frac{1.4}{7.7\pi}\sin\left(7.7\pi \cdot X_k^n\right)\left(1 - X_k^n\right)\right), 1\right), \text{if } X_k^n \geq 0.5. \end{cases} \tag{39}$$

where Y_{k+1}^n are chaotic sequences for the interval $[0, 1]$; $n = 1, 2, 3 \cdots, N$; and $k = 1, 2, 3 \cdots, D - 1$.

The initial solution dimension distribution plots and histograms of the initial solution dimension distributions before and after improvement are shown in Figure 4. Setting the spatial dimension $D = 5000$, as shown in Figures 4(a) and 4(b), it is clear that the chaotic values of the logistic-circle chaotic mapping are more evenly distributed. Therefore, the improved logistic-circle chaotic mapping is used to initialize the population and enhance the diversity of the population, which in turn enhances the optimization ability of the algorithm.

An inverse mapping is then performed to obtain the initial position of the population, as shown in the following equation:

$$X_d^n = Y_k^n(ub(N, D) - lb(N, D)) + lb(N, D). \tag{40}$$

To extend the global search effectively, individuals are guided to explore other positions to increase the diversity of the population and improve the local search capability of the algorithm. The leader positions are updated using an adaptive disturbance strategy.

$$X_d^1 = \begin{cases} F_d + c_1\left(c_2 + 0.5r_1\right)F_d\, c_1 \geq 0.8, \\ F_d - c_1\left(c_2 + 0.5r_1\right)F_d\, c_1 < 0.8. \end{cases} \tag{41}$$

$$c_1 = \begin{cases} 2e^{-(4l/L)^2}, & t \geq \frac{L}{2}, \\ 2e^{-(4(T-l)/L)^2}, & t < \frac{L}{2}, \end{cases} \tag{42}$$

where r_1 is a random distribution on $(0, 1)$, causing a perturbation deviation from the individual optimum of the salp swarm, causing a change in the direction of individual movement, and preventing individuals from falling into a local optimum.

To validate the performance of logistic-circle and disturbance-adaption salp swarm algorithm (LDSSA), a comparison was made with SSA. Validation was carried out against the benchmark functions in Table 1 by setting the maximum number of iterations and population size. Among them, F1–F3 are single-peaked functions with only one global optimum, which can well reflect the convergence performance of the algorithm, and F4–F6 are multipeaked

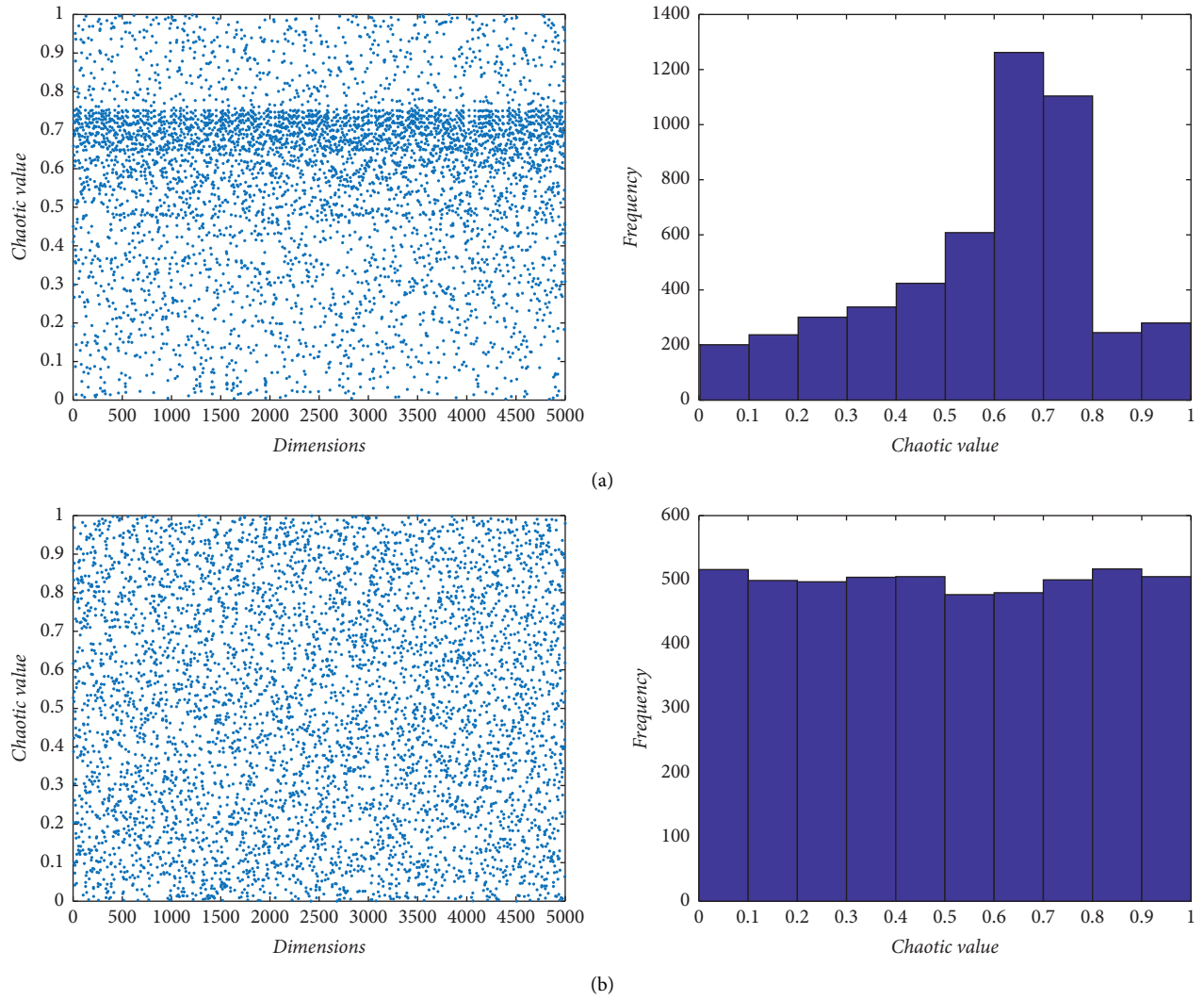

Figure 4: Plot of initial solution dimension distribution and histogram of initial solution dimension distribution for the two chaotic mappings. (a) Circle. (b) Logistic-circle.

functions with multiple local optima, which can well reflect the ability of the algorithm to jump out of the local optimum.

Figure 5 shows that on the single-peaked high-dimensional solution problems, LDSSA converges within 550 generations, proving that LDSSA has good convergence accuracy and convergence speed. On the problem of solving multipeak functions, the convergence curve of LDSSA shows a stepwise decline as shown in Figures 5(d) and 5(f). The iterative process falls into the local optimum several times; however, LASSA is able to jump out of the current local optimum well, which also proves the effectiveness of the leader's adaptive perturbation update strategy.

4.2. Model Calibration and Validation. Different parameter settings represent different driving behaviors in the car-following model, and there are differences in the traffic scenarios to which they are adapted. In this study, the parameters in the improved DIDM-CSCL model were parameter calibrated using the following data during vehicle acceleration and deceleration on urban roads. The DIDM-CSCL model calibration results are listed in Table 2, with the relevant parameters $\gamma = 0.31$ and $\mu = 0.28$.

To verify the superiority of the improved DIDM-CSCL and IDM in terms of error accuracy, the trajectory fitting results of the two models were compared with the actual rear vehicle trajectory data. The mean square error, mean absolute error, and goodness of fit were calculated to determine whether the improved model had significantly improved in terms of trajectory fitting accuracy. As shown in Figure 6 and Table 3, the improved DIDM-CSCL model at the sum time improved the error accuracy compared to the original model and 2.2% in fitting accuracy compared to the original model, thus verifying that the improved DIDM-CSCL model is better than the original IDM in fitting accuracy.

Table 1: Benchmark functions.

Name	Function	Dimension	Definition field
F1	Sphere	200	[−100, 100]
F2	Schwefel 1.2	200	[−100, 100]
F3	Rosenbrock	30	[−30, 30]
F4	Rastrigin	100	[−5.12, 5.12]
F5	Griewank	100	[−100, 100]
F6	Kowalik	4	[−5, 5]

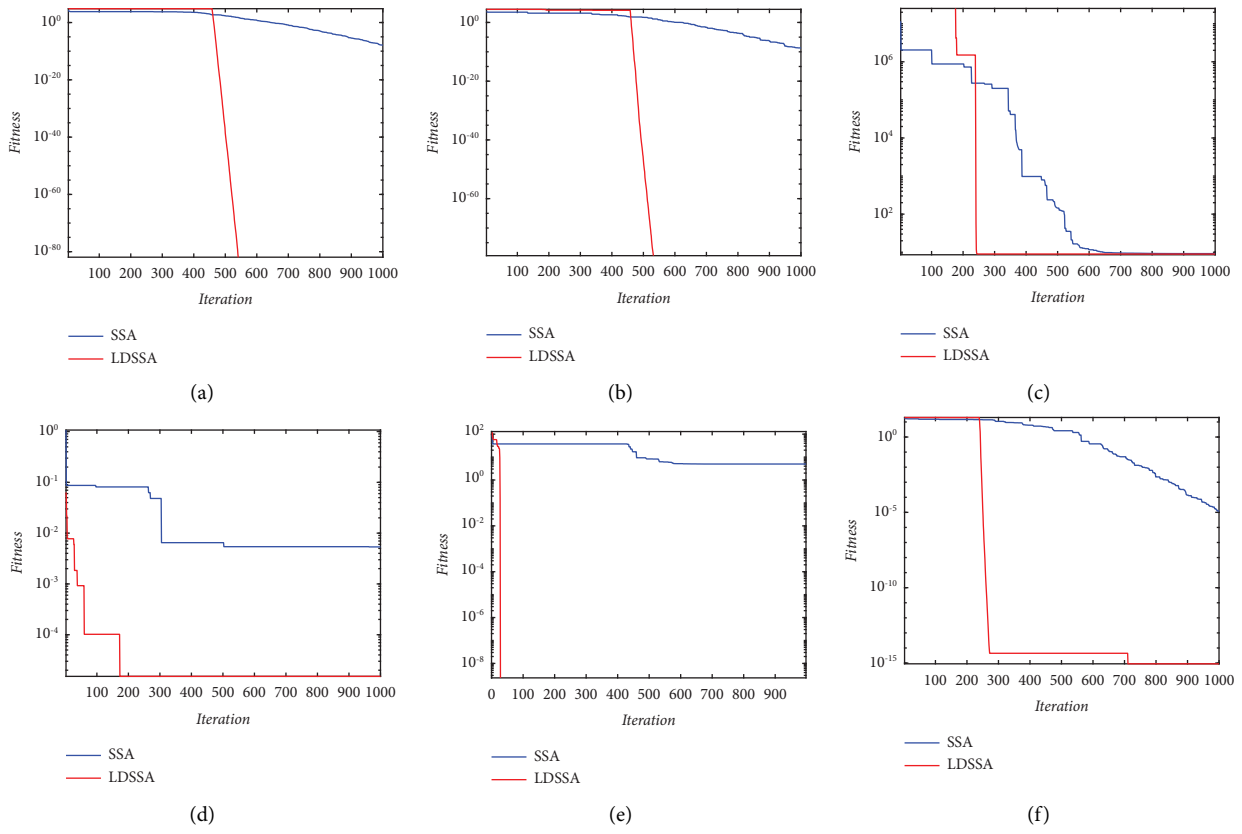

Figure 5: Comparison of convergence curves of different algorithms. (a) F1. (b) F2. (c) F3. (d) F4. (e) F5. (f) F6.

Table 2: Calibration results of DIDM-CSCL model parameters.

Parameters	Description	Boundaries	Value
a_0	Maximum acceleration	[0.1, 5]	2.2
b	Comfortable deceleration	[0.1, 5]	1.6
s_0	Minimum headway	[0.1, 10]	3.5
T	Safe time headway	[0.1, 5]	1.6
γ	Collision quantization sensitivity factor	[0.1, 1]	0.31
μ	Speed limit sensitivity factor	[0.1, 1]	0.28

5. Numerical Simulation

To investigate the dynamic performance of the improved DIDM-CSCL model, we used the DIDM-CSCL model to simulate the acceleration motion of vehicles when the traffic signal changes from red to green and to test some properties of the improved IDM. When the traffic signal is red, 10 vehicles are in a line, all vehicles are at rest, and the interval between vehicles is 2.5 m. At $t = 0$, the traffic signal turns green and the vehicles start to move. To compare the improved DIDM-CSCL model with the original model, we set the parameters for both models as shown in Table 2, where the desired speed and speed limits are 10 m/s and the delay time is 0.15 s.

Numerical simulations using the two models were run to obtain the acceleration, speed, and position changes as shown in Figures 7–9. It can be seen from the figure that the acceleration maximum value in the DIDM-CSCL model was larger than that of the IDM and

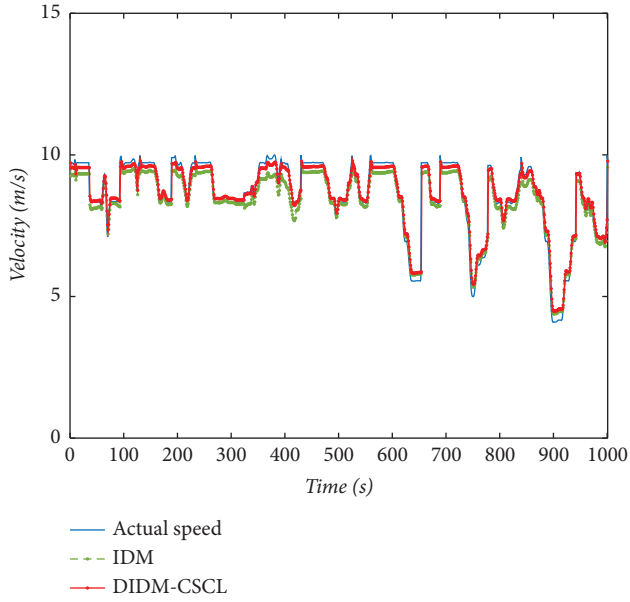

Figure 6: DIDM-CSCL and IDM rear vehicle fitted trajectory data curves.

Table 3: Fitting error data corresponding to the two models.

Mode	ME	MAE	RMSE	R^2 (%)
IDM	0.198	0.283	0.384	95.4
DIDM-CSCL	0.109	0.253	0.356	97.6

the acceleration process used less time than the IDM. The DIDM-CSCL model of the speed distribution converged faster to the maximum value than did the original IDM, which is consistent with the real movement of vehicles at intersections. After the traffic light turns from red to green, vehicles generally increase their speed to reach maximum speed as quickly as possible under safe conditions to cross the intersection.

To investigate the effects of sensitive collision factors and speed limits on the stability of the following traffic, the simulation was carried out on a 400 m long circular road with $N = 100$ vehicles evenly spaced and a simulation step size of 0.01 s, with other parameters kept constant.

Figure 10 shows the headway distribution of 100 vehicles at 500 s for the DIDM-CSCL model in the case of $\mu = 0$ with γ taking the values 0, 0.1, 0.2, and 0.31. Figure 11 shows the headway distribution of 100 vehicles for the DIDM-CSCL model at 500 s for the case $\gamma = 0$ with μ taking the values 0, 0.1, 0.2, and 0.28. The comparison shows that changing the value of γ or μ changes the space headway of the following traffic when all the other conditions are consistent. In particular, the amplitude of the headway oscillation was greatest at $\gamma = 0$ and $\mu = 0$, with a peak-to-trough difference of 0.536 m at 500 s. The peak-to-trough difference was 0.31 m for $\gamma = 0.31$ and $\mu = 0.28$. The experiments show that the introduction of a collision sensitivity factor and speed limit information into the traffic model is beneficial to the stability of the traffic flow.

Figures 12(a)–12(d) show the velocity time-space diagrams of the perturbation propagating in the following traffic for different values of γ and μ. When $\gamma = 0$ and $\mu = 0$, the model is the IDM; under the disturbance action, many fold bands appear in the velocity time-space diagram of the traffic flow, indicating that the velocity in the traffic flow is constantly changing. With the passage of time, the disturbance propagates in the following traffic flow, eventually affecting the stability of the traffic system, causing the entire system to be in an unstable state (such as causing traffic jams). The dispersion of the disturbance was relatively poor. In Figures 12(b)–12(d), by gradually increasing the values of γ and μ, the fluctuation in the velocity of the following traffic began to decrease. At $\gamma = 0.31$ and $\mu = 0.28$, the speed leveled off, indicating that the disturbance was controlled or even dissipated in the following traffic. The above numerical simulation experiments and analysis results show that the stability of traffic flow can be further improved by introducing collision-sensitive factors and speed limit information into the IDM.

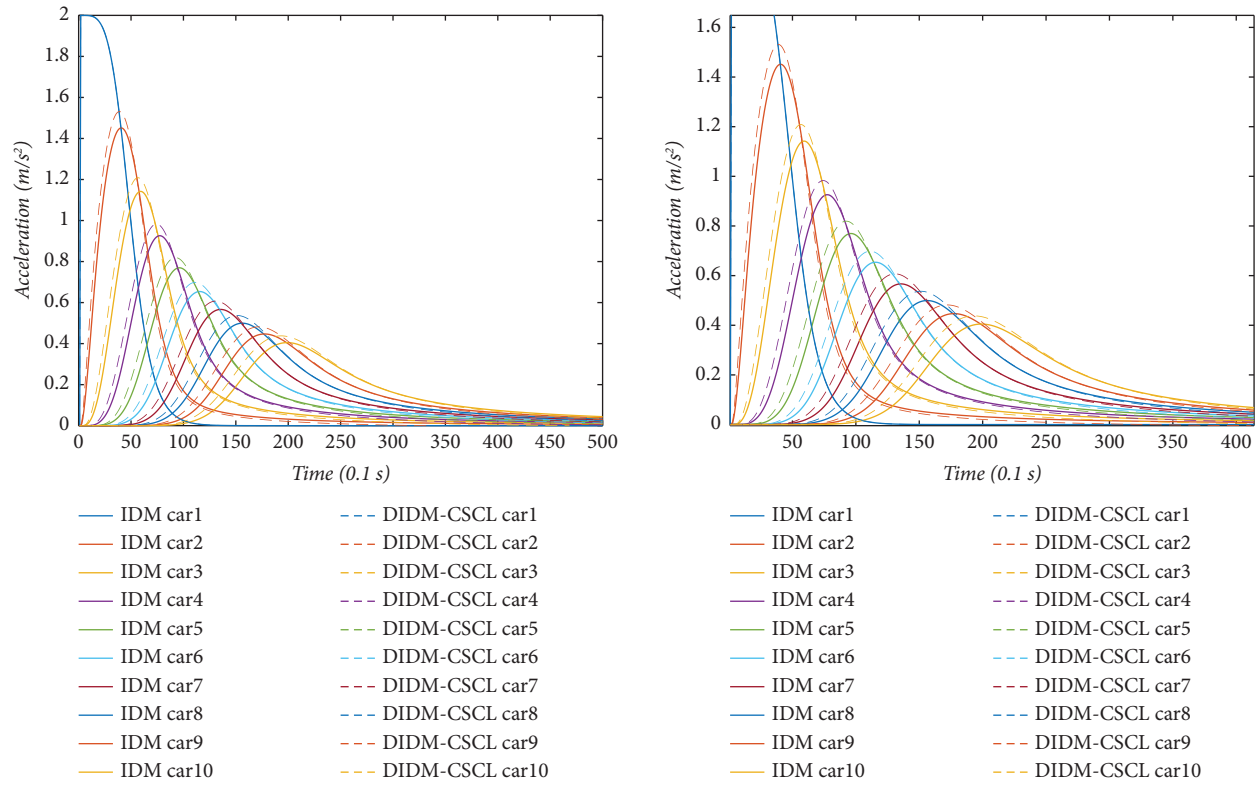

Figure 7: Vehicle acceleration distribution curve and its partial enlargement (solid line: IDM; dashed line: DIDM-CSCL).

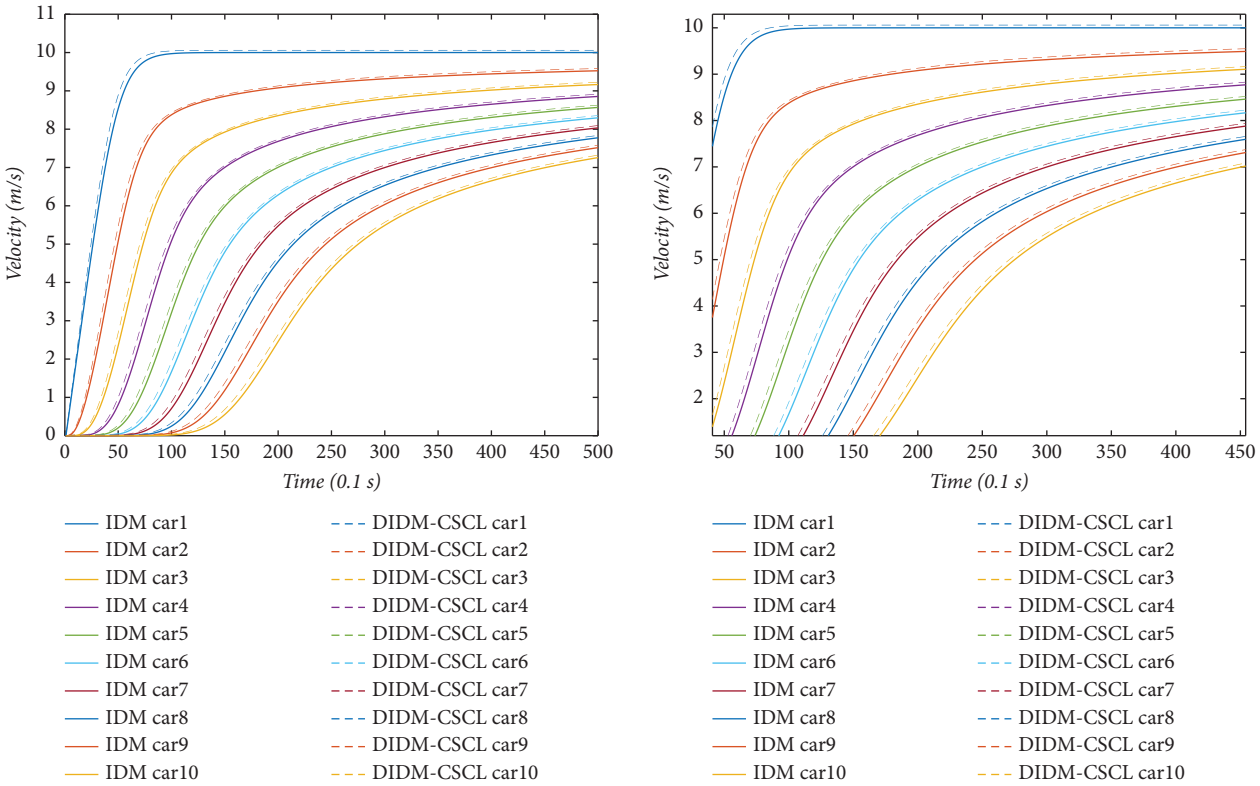

Figure 8: Vehicle speed distribution curve and its partial enlargement (solid line: IDM; dashed line: DIDM-CSCL).

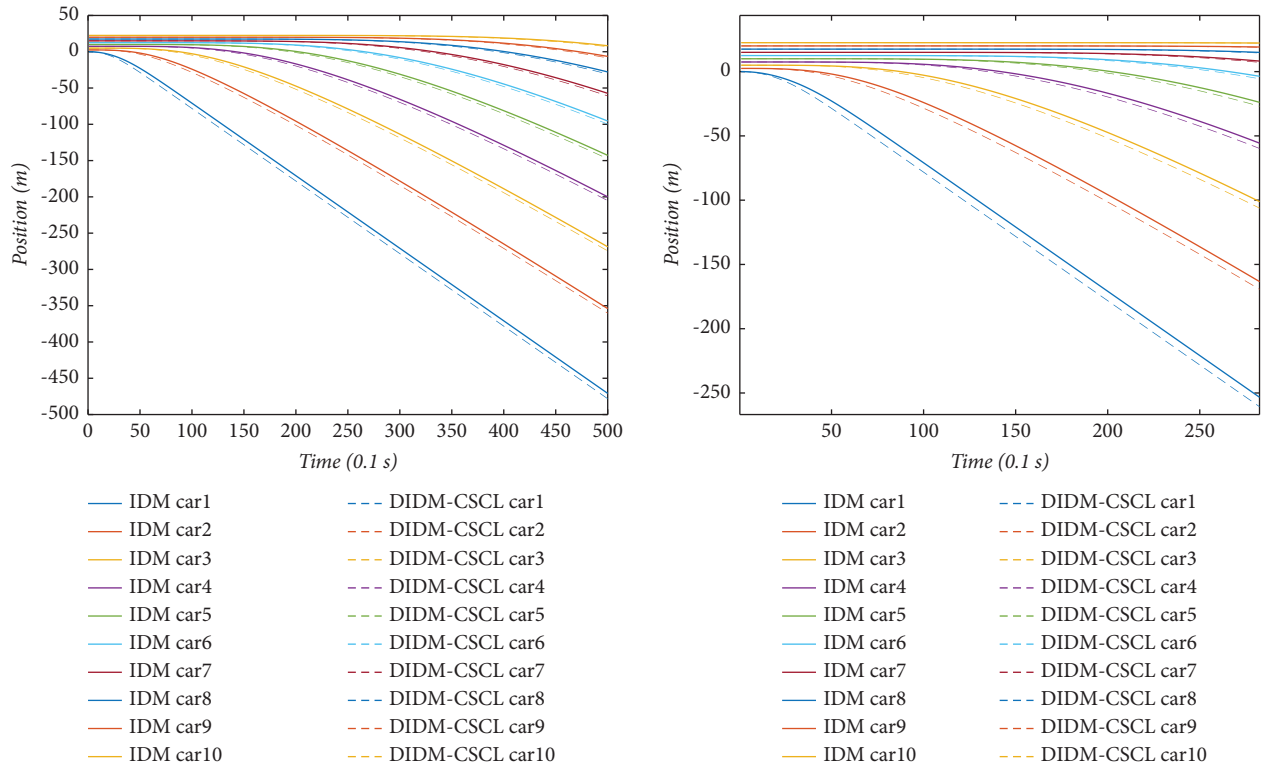

Figure 9: Vehicle position distribution curve and its partial enlargement (solid line: IDM; dashed line: DIDM-CSCL).

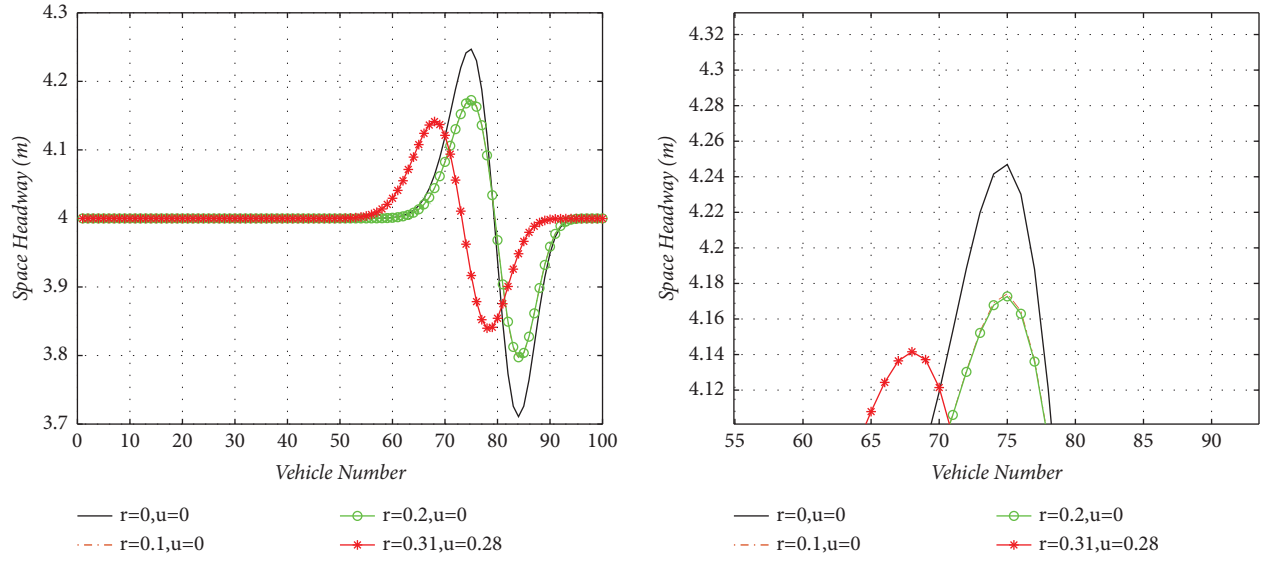

Figure 10: Comparison of the different space headways of different γ at 500 s and its partial enlargement.

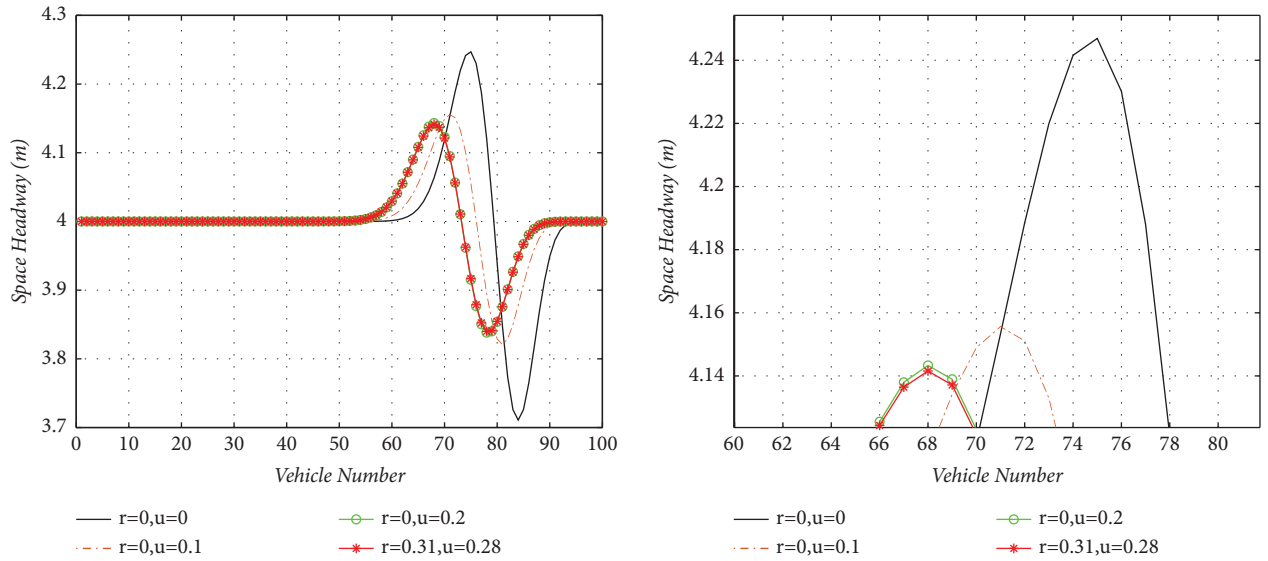

FIGURE 11: Comparison of the different space headways of different μ at 500 s and its partial enlargement.

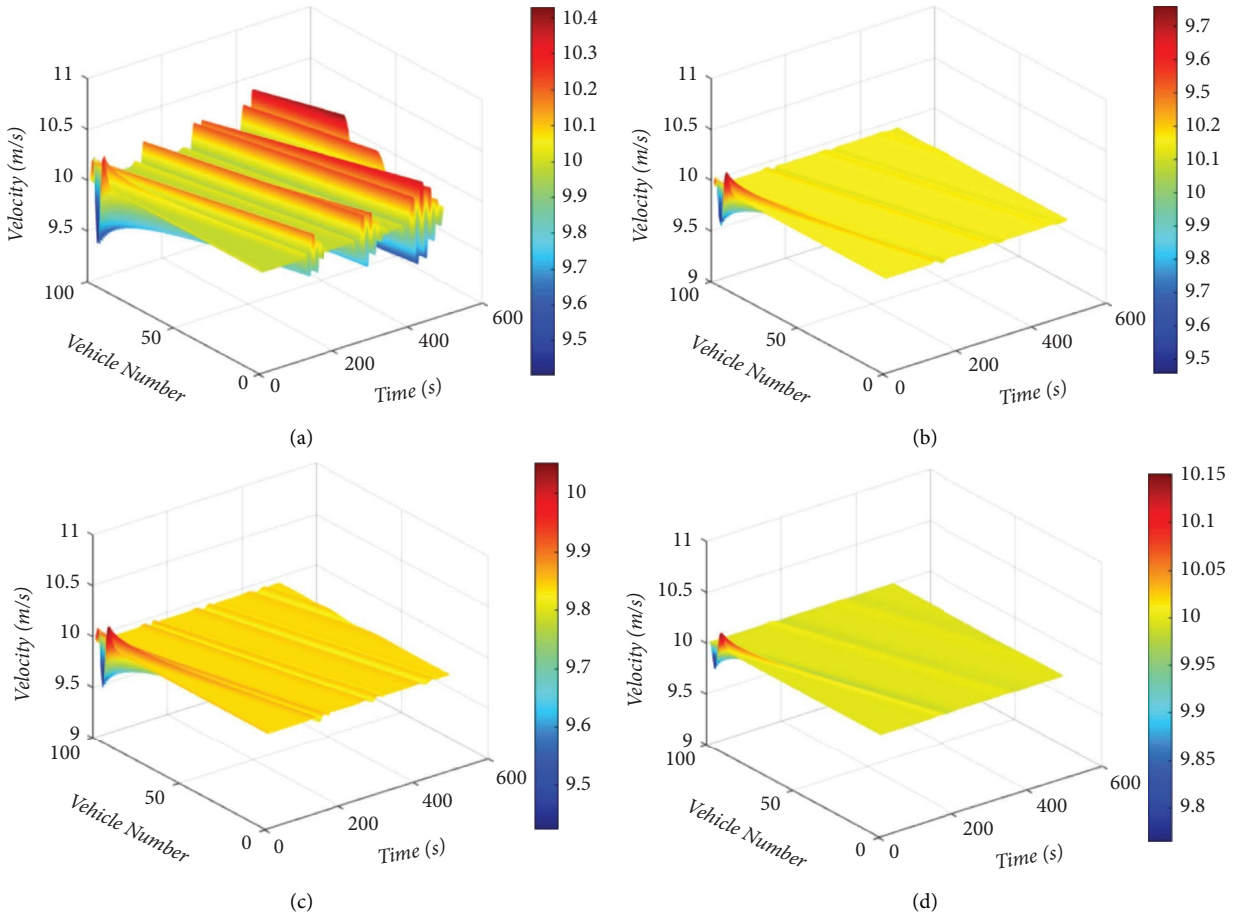

FIGURE 12: Time-space variation of velocity for different values of γ and μ. (a) $\gamma = 0, \mu = 0$. (b) $\gamma = 0, \mu = 0.1$. (c) $\gamma = 0.1, \mu = 0$. (d) $\gamma = 0.31, \mu = 0.28$.

6. Conclusion

In a connected environment, this paper proposed a DIDM-CSCL model based on the IDM, which was improved by introducing information such as a time delay for reception and processing, collision risk quantification factor, and mandatory speed limit. The stability conditions of the DIDM-CSCL model were obtained through a linear stability analysis. The results showed that considering information such as the collision risk quantization factor and mandatory speed limit further improved the stability of traffic flow and effectively suppressed traffic congestion. The model was also calibrated using real vehicle data from urban roads, the optimal parameters of the model were obtained through error analysis, and the fitting accuracies of the two models were compared and analyzed. The results showed that the improved DIDM-CSCL model outperformed the original IDM in terms of the fitting accuracy.

The numerical simulation showed that the DIDM-CSCL model outperformed the IDM in terms of the acceleration, velocity, and headway distribution of the vehicle, which is more in line with the actual situation. However, owing to the complexity of the traffic system, it is necessary to further expand the calibration sample and calibrate the model parameters more accurately. Additionally, to meet the actual situational requirements and needs of the current development of autonomous driving and other technologies, it is necessary to consider following behavior under the influence of multiple vehicles in front and behind. Future work is needed to address the following areas: (1) vehicles in heterogeneous traffic flows do not follow the same model and (2) nonuniform initial conditions need to be simulated to investigate the effectiveness of DIDM-CSCL in complex environments.

Data Availability

The data are not publicly available due to privacy. The car-following data of CVs used to support the findings of this study may be released upon request to the Joint Laboratory for Internet of Vehicles, Ministry of Education-China Mobile Communications Corporation, who can be contacted at 86-29-82334763.

Conflicts of Interest

The authors declare that they have no conflicts of interest.

Acknowledgments

This research was funded by the National Natural Science Foundation of China (Grant no. 52172380).

References

[1] H. Zhao, R. He, and C. Ma, "An extended car-following model at signalised intersections," *Journal of Advanced Transportation*, vol. 2018, p. 26, 2018.

[2] D. C. Gazis, R. Herman, and R. W. Rothery, "Nonlinear follow-the-leader models of traffic flow," *Operations Research*, vol. 9, no. 4, pp. 545–567, 1961.

[3] E. Kometani and T. Sasaki, "Dynamic behavior of traffific with a nonlinear spacing-speed relationship," *Theory of Traffic Flow*, pp. 105–119, 1959.

[4] R. M. Michaels, "Perceptual factors in car following," in *Proceedings of the Second International Symposium on the Theory of Traffific Flow*, pp. 44–59, London, UK, June 1963.

[5] S. Kikuchi and P. Chakraborty, "Car following model based on a fuzzy inference system," *Transportation Research Record*, vol. 1194, pp. 82–91, 1992.

[6] M. Bando, K. Hasebe, A. Nakayama, A. Shibata, and Y. Sugiyama, "Dynamical model of traffic congestion and numerical simulation," *Physical Review*, vol. 51, no. 2, pp. 1035–1042, 1995.

[7] M. Talal, K. N. Ramli, A. A. Zaidan, B. Zaidan, and F. Jumaa, "Review on car-following sensor based and data-generation mapping for safety and traffic management and road map toward ITS," *Vehicular Communications*, vol. 25, 2020.

[8] M. Treiber, A. Hennecke, and D. Helbing, "Congested traffic states in empirical observations and microscopic simulations," *Physical Review*, vol. 62, no. 2, pp. 1805–1824, 2000.

[9] X. Q. Chen, W. J. Xie, J. Shi, and Q. X. Shi, "Perturbation and stability analysis of the multi-anticipative intelligent driver model," *International Journal of Modern Physics C*, vol. 21, no. 05, pp. 647–668, 2010.

[10] M. Treiber, A. Kesting, and D. Helbing, "Delays, inaccuracies and anticipation in microscopic traffic models," *Physica A: Statistical Mechanics and Its Applications*, vol. 360, no. 1, pp. 71–88, 2006.

[11] R. Hoogendoorn, B. Van Arem, and S. Hoogendoorn, "Incorporating driver distraction in car-following models: applying the TCI to the IDM," in *Proceedings of the 16th International IEEE Conference on Intelligent Transportation Systems (ITSC 2013)*, pp. 2274–2279, The Hague, Netherlands, October 2013.

[12] M. Saifuzzaman and Z. Zheng, "Incorporating human-factors in car-following models: a review of recent developments and research needs," *Transportation Research Part C: Emerging Technologies*, vol. 48, pp. 379–403, 2014.

[13] R. Fuller, "Towards a general theory of driver behaviour," *Accident Analysis and Prevention*, vol. 37, no. 3, pp. 461–472, 2005.

[14] M. Saifuzzaman, Z. Zheng, M. Mazharul Haque, and S. Washington, "Revisiting the Task–Capability Interface model for incorporating human factors into car-following models," *Transportation Research Part B: Methodological*, vol. 82, pp. 1–19, 2015.

[15] X. Xiao, M. Jiang, J. Wen, and C. Wu, "A novel car-following model considering conditional heteroskedasticity of acceleration fluctuation and driving force," *Journal of Intelligent and Fuzzy Systems*, vol. 34, no. 4, pp. 2301–2311, 2018.

[16] F. Zong, M. Wang, M. Tang, X. Li, and M. Zeng, "An improved intelligent driver model considering the information of multiple front and rear vehicles," *IEEE Access*, vol. 9, pp. 66241–66252, 2021.

[17] A. Sharma, Z. Zheng, A. Bhaskar, and M. M. Haque, "Modelling car-following behaviour of connected vehicles with a focus on driver compliance," *Transportation Research Part B: Methodological*, vol. 126, pp. 256–279, 2019.

[18] T. Li, D. Ngoduy, F. Hui, and X. Zhao, "A car-following model to assess the impact of V2V messages on traffic dynamics," *Transportation Business: Transport Dynamics*, vol. 8, no. 1, pp. 150–165, 2020.

[19] Y. Huang, X. Yan, X. Li, and J. Yang, "Using a multi-user driving simulator system to explore the patterns of vehicle

fleet rear-end collisions occurrence under different foggy conditions and speed limits," *Transportation Research Part F: Traffic Psychology and Behaviour*, vol. 74, pp. 161–172, 2020.

[20] B. Ponnu and B. Coifman, "When adjacent lane dependencies dominate the uncongested regime of the fundamental relationship," *Transportation Research Part B: Methodological*, vol. 104, pp. 602–615, 2017.

[21] M. Treiber and A. Kesting, "The Intelligent Driver Model with stochasticity – new insights into traffic flow oscillations," *Transportation Research Part B: Methodological*, vol. 117, pp. 613–623, 2018.

[22] Y. Zheng, G. Zhang, Y. Li, and Z. Li, "Optimal jam-absorption driving strategy for mitigating rear-end collision risks with oscillations on freeway straight segments," *Accident Analysis and Prevention*, vol. 135, 2020.

[23] Y. Li, H. Wang, W. Wang, L. Xing, S. Liu, and X. Wei, "Evaluation of the impacts of cooperative adaptive cruise control on reducing rear-end collision risks on freeways," *Accident Analysis and Prevention*, vol. 98, pp. 87–95, 2017.

[24] Y. Wu, M. Abdel Aty, L. Wang, and M. S. Rahman, "Combined connected vehicles and variable speed limit strategies to reduce rear-end crash risk under fog conditions," *Journal of Intelligent Transportation Systems*, vol. 24, no. 5, pp. 494–513, 2020.

[25] X. Wang, X. Zhang, F. Guo, Y. Gu, and X. Zhu, "Effect of daily car-following behaviors on urban roadway rear-end crashes and near-crashes: a naturalistic driving study," *Accident Analysis and Prevention*, vol. 164, 2022.

[26] Z. Yao, R. Hu, Y. Jiang, and T. Xu, "Stability and safety evaluation of mixed traffic flow with connected automated vehicles on expressways," *Journal of Safety Research*, vol. 75, pp. 262–274, 2020.

[27] K. D. Kusano, R. Chen, J. Montgomery, and H. C. Gabler, "Population distributions of time to collision at brake application during car following from naturalistic driving data," *Journal of Safety Research*, vol. 54, pp. 95-e29–104, 2015.

[28] Y. Li, L. Xing, W. Wang, H. Wang, C. Dong, and S. Liu, "Evaluating impacts of different longitudinal driver assistance systems on reducing multi-vehicle rear-end crashes during small-scale inclement weather," *Accident Analysis and Prevention*, vol. 107, pp. 63–76, 2017.

[29] M. Rahman, M. Abdel-Aty, and Y. Wu, "A multi-vehicle communication system to assess the safety and mobility of connected and automated vehicles," *Transportation Research Part C: Emerging Technologies*, vol. 124, 2021.

[30] X. Li and J. Q. Sun, "Effects of vehicle–pedestrian interaction and speed limit on traffic performance of intersections," *Physica A: Statistical Mechanics and Its Applications*, vol. 460, pp. 335–347, 2016.

[31] J. Sun, Z. Zheng, and J. Sun, "Stability analysis methods and their applicability to car-following models in conventional and connected environments," *Transportation Research Part B: Methodological*, vol. 109, pp. 212–237, 2018.

[32] M. Montanino and V. Punzo, "On string stability of a mixed and heterogeneous traffic flow: a unifying modelling framework," *Transportation Research Part B: Methodological*, vol. 144, pp. 133–154, 2021.

[33] J. Sun, Z. Zheng, and J. Sun, "The relationship between car following string instability and traffic oscillations in finite-sized platoons and its use in easing congestion via connected and automated vehicles with IDM based controller," *Transportation Research Part B: Methodological*, vol. 142, pp. 58–83, 2020.

[34] Y. Li, B. Chen, H. Zhao et al., "A car-following model for connected and automated vehicles with heterogeneous time delays under fixed and switching communication topologies," *IEEE Transactions on Intelligent Transportation Systems*, vol. 23, no. 9, pp. 14846–14858, 2022.

[35] S. Mirjalili, A. H. Gandomi, S. Z. Mirjalili, S. Saremi, H. Faris, and S. M. Mirjalili, "Salp Swarm Algorithm: a bio-inspired optimizer for engineering design problems," *Advances in Engineering Software*, vol. 114, pp. 163–191, 2017.

[36] L. Abualigah, M. Shehab, M. Alshinwan, and H. Alabool, "Salp swarm algorithm: a comprehensive survey," *Neural Computing and Applications*, vol. 32, no. 15, pp. 11195–11215, 2020.